AIAA JOURNAL
Vol. 41, No. 6, June 2003

Postbuckling of Stiffened Panels Using Strut, Strip, and Finite Element Methods

M. Lillico,* R. Butler,† and G. W. Hunt‡
University of Bath, Bath, England BA2 7AY, United Kingdom
and
A. Watson§ and D. Kennedy¶
Cardiff University, Cardiff, Wales CF24 0YF, United Kingdom

Postbuckling results are presented for isotropic stiffened panels loaded in compression. Comparisons are made between single-bay and double-bay finite element (FE) models (where "bay" denotes a repeating portion, between supports, in the load/length direction) and a new strut model, following a Shanley-type approach, for single-bay and multibay panels. The strut model has been incorporated within the strip program VIPASA with CONstraints and OPTimization (VICONOPT) to design a multibay example panel with postbuckling reserve of strength in its skins, assuming linear elastic material properties. The panel has been shown by VICONOPT to have a stiffener buckling failure mode when an overall sinusoidal imperfection causing increased stiffener compression is present. The failure is confirmed by the double-bay FE model, which is shown to be an imperfect representation of the multibay case. Single-bay analysis using the strut model shows good agreement with the single-bay FE results. The VICONOPT code is able to design a metallic panel of realistic dimensions and loading using 50 strip elements (compared with the 9600 shell elements required by the finite element model) but cannot correctly account for material nonlinearity. The important phenomenological difference between postbuckling of single-, double-, and multibay panel models are indicated.

Nomenclature

EI	=	bending rigidity of strut/panel
e_{sk}	=	offset between load and neutral axis
l	=	length of panel/strut
P	=	axial load
P_E	=	Euler or overall buckling load
$P_{E,sk}$	=	Euler or overall buckling load of skin-buckled panel
P_{sk}	=	skin buckling load
r_L	=	factor of ultimate design load at which local skin buckling occurs
r_s	=	postbuckling to prebuckling stiffness ratio
$v(x)$	=	deflection of strut
δ	=	midlength deflection of strut
δ_0	=	amplitude of initial imperfection
$\delta_{0,sk}$	=	amplitude of initial imperfection for skin-buckled panel
λ	=	half-wavelength of buckling mode

I. Introduction

STIFFENED panels, used extensively within the aerospace industry, can have a considerable postbuckling reserve of strength in their skins, enabling them to remain in stable equilibrium under loads in excess of their critical local buckling load. By allowing such designs to buckle in a stable manner, for example, between limit and ultimate design loads, it is possible to save a significant amount of mass compared to designs for which buckling is not permitted.

Many different techniques[1–3] have been developed to model the buckling and postbuckling behavior of stiffened panels. These include finite-strip methods and exact strip methods for preliminary analysis/design and finite element (FE) methods that use shell elements and are suitable for detailed analysis/design. All such techniques make assumptions about the loading distribution in the structure, especially when modeling the panel as an individual component, separate from the complete structure, for example, the wing box.

The preliminary design program VICONOPT[3] (VIPASA with CONstraints and OPTimization) represents plates as strips for buckling and postbuckling analysis but uses strut theory to account for out-of-plane load distribution. The exact strip theory considers the panel to be infinitely long (multibay) with transverse ribs at longitudinal spacing l, thus modeling a panel of length l that is simply supported with warping of the entire cross section allowed. For this multibay case uniform end strain is assumed for the whole panel cross section throughout loading, so that as the skin buckles, and its stiffness is reduced, the point at which the load is applied effectively moves away from the skin to the new (buckled) neutral axis position. As previously shown,[4] these boundary conditions do not arise when considering a single-bay FE model, simply supported over length l. Here, the end-load position remains fixed when the skin buckles, so that an offset between load and new neutral axis position causes the panel to always fail on its skin side, regardless of the direction of an overall sinusoidal imperfection; experimental tests on single-bay panels[4] have shown this to be a stable form of failure. The former multibay case has an increased stiffener load after skin buckling compared with the single-bay case and therefore can lead to stiffener-induced failure of the panel that could be highly unstable.[5] The multibay approach is a better representation of an actual aircraft wing box, where panels are continuous over ribs.

In this paper the strut theory, used to describe the load vs out-of-plane deflection relationship before and after initial skin buckling for single-bay and multibay conditions, is developed first. The aim

Received 3 April 2001; presented as Paper 2001-1329 at the 42nd Structures, Structural Dynamics, and Materials Conference, Seattle, WA, 16–19 April 2001; revision received 30 September 2002; accepted for publication 14 January 2003.

*Research Officer, Department of Mechanical Engineering; currently Professional Engineer, Airbus UK, Filton, Bristol, England BS99 7AR, United Kingdom.
†Senior Lecturer in Aerospace Structures, Department of Mechanical Engineering; r.butler@bath.ac.uk.
‡Professor of Structural Mechanics, Department of Mechanical Engineering.
§Senior Research Associate, Cardiff School of Engineering. Member AIAA.
¶Senior Lecturer, Cardiff School of Engineering. Senior Member AIAA.

is then to compare the effects of these different boundary conditions on the initial and postbuckling behavior of an optimized J-stiffened panel. This panel was designed using a recently developed version of VICONOPT[6,7] that estimates the postbuckled stiffnesses of the buckled plates. Comparisons will be made between results given by VICONOPT and a series of ABAQUS[8] (FE) single-bay and double-bay panel models, where the double-bay model is an approximation of the multibay case.

II. Strut Theory and Shanley Model

Nonlinear, out-of-plane deflections arise at the midlength of a compressively loaded panel when either an initial sinusoidal imperfection of amplitude δ_0 is present (Fig. 1a) or some of the compressive load is offset from the neutral axis of the panel (Fig. 1b). Strut theory is used in VICONOPT to calculate these deflections; it is also used in Sec. IV.D to compare results for single- and multibay cases.

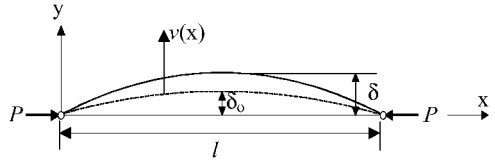

Fig. 1a Strut model for initial sinusoidal imperfection δ_0 when $P < P_{sk}$.

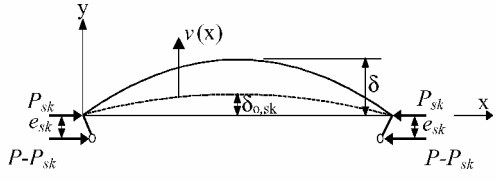

Fig. 1b Strut model for initial sinusoidal imperfection $\delta_{0,sk}$ and offset load when $P \geq P_{sk}$.

The basis for this theory follows from the Shanley model, which can be adapted to illustrate the pre- and postbuckling behavior of stiffened panels.[9] The sudden reduction in stiffness in the skin of a stiffened panel that occurs when a critical skin-buckling load is reached also occurs in the Shanley model, where part of the model is made to reduce in stiffness at a critical load. This model is briefly described here to introduce some of the concepts that will later be applied to the strut equations of Sec. II.B.

A. Shanley Model

Figure 2a shows the Shanley model used to represent the stiffened panel, with one spring representing the stiffeners and the other representing the skin. In the case shown here the system is initially loaded along its neutral axis, and no initial imperfection is present. For simplicity, it has been assumed that both skin and stiffener springs initially have stiffness k. At a (critical) total load of $P = P_{sk}$, that is, when the load in the skin is $P_{sk}/2$, the stiffness of the skin is reduced to $r_s k$ to approximate the effect of local buckling (Fig. 2b). For loads above P_{sk}, this reduced stiffness results in rotation of the structure, indicated by θ in Fig. 2a. Hence, at $P = P_{sk}$ the response of the system switches from equilibrium path OA on Fig. 2c to path AB. Such a switch introduces an effective negative (initial) imperfection θ_0 to the reduced stiffness structure, the value of which depends on both the reduced spring stiffness and the critical load P_{sk}. This value of θ_0 can be obtained by considering the unloaded system of Fig. 2d, which has skin stiffness $r_s k$, and ΔL is the extension required to make the imperfect equilibrium path $O'B$ pass through A.

After the skin reduces stiffness there is no sudden jump in rotation θ despite a sudden change in the position of the neutral axis, resulting in a sudden offset between it and the position at which the load is applied. The reduction in stiffness of one of the springs only affects the additional load applied above P_{sk}, and thus the rotation of the structure is zero at P_{sk} and smoothly increases with increment of load above P_{sk}. This behavior is similar to the case of the stiffened panel, loaded along its original neutral axis both before and after skin buckling. Here there is also a sudden change in stiffness when a critical load is reached, and, like the Shanley model, the change in

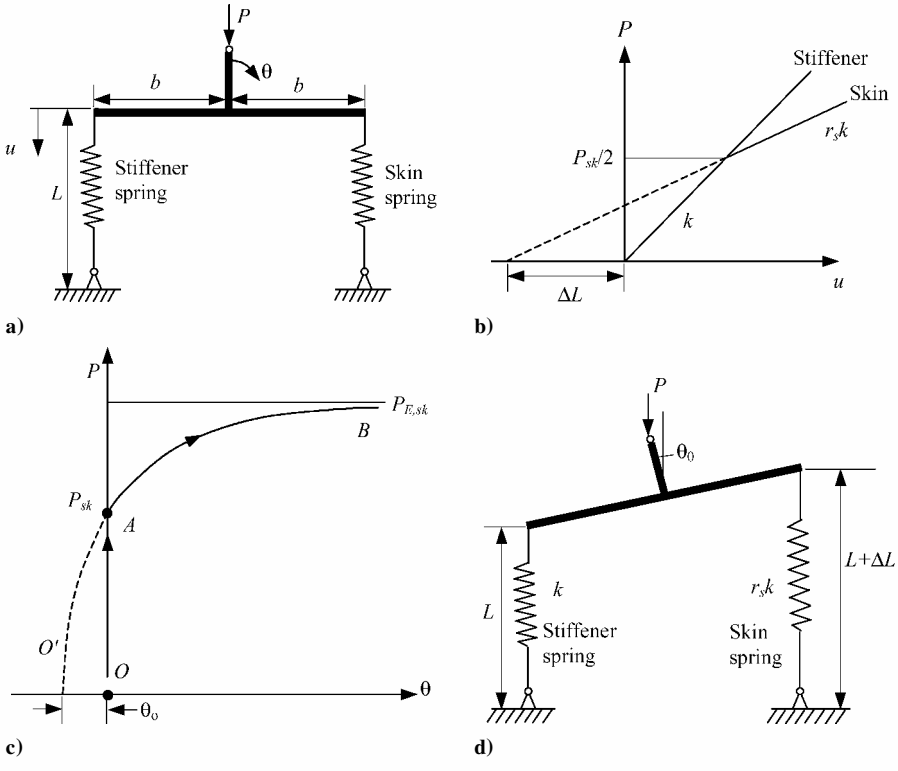

Fig. 2 Shanley model of stiffened panel: a) initially perfect case for $P < P_{sk}$ with skin and stiffener stiffness both k; see panel b, giving equilibrium path OA in panel c; d) initially imperfect case for $P > P_{sk}$ with skin stiffness reduced to $r_s k$; see panel b, giving equilibrium path $O'AB$ in panel c.

stiffness only affects the extra load applied above the critical load. Hence, using these ideas, strut equations are now developed to form a simplified model of the pre- and postbuckled behavior of a stiffened panel.

B. Strut Theory

For loads below the skin-buckling load P_{sk}, there is no offset between load and neutral axis, and the midlength ($x = l/2$) deflection δ (see Fig. 1a) is given by the following well-known equation:

$$\delta = \frac{\delta_0}{(1 - P)/P_E} \tag{1}$$

where

$$\delta = v(l/2) + \delta_0 \tag{2}$$

After the skin has buckled, that is, $P \geq P_{sk}$, the situation is more complex, and models can be developed to describe single- and multibay cases. For the single-bay case, where the load remains applied at the neutral axis of the original (unbuckled) panel, an offset e_{sk} is introduced to represent the offset associated with the load above P_{sk}, (see Fig. 1b). Hence, the following differential equation can be obtained in terms of $v(x)$:

$$\mathrm{EI}\frac{\mathrm{d}^2 v}{\mathrm{d}x^2} = P_{sk}e_{sk} - P\left(e_{sk} + v + \delta_0 \sin\frac{\pi x}{l}\right) \tag{3}$$

Solving Eq. (2) for the midlength ($x = l/2$) deflection δ gives

$$\delta = \frac{\delta_{0,sk}}{1 - (P/P_{E,sk})} + e_{sk}\left(1 - \frac{P_{sk}}{P}\right)\left[\sec\left(\frac{\pi}{2}\sqrt{\frac{P}{P_{E,sk}}}\right) - 1\right] \tag{4}$$

Values of $P_{E,sk}$ and e_{sk} can be calculated by assuming that the elastic modulus of the skin is reduced by factor r_s following buckling. The amplitude of the initial imperfection for the skin-buckled panel $\delta_{0,sk}$, which can be thought of as being similar to θ_0 for the preceding Shanley model, is given by equating Eqs. (1) and (4) with $P = P_{sk}$. Hence,

$$\delta_{0,sk} = \frac{\delta_0}{(1 - P_{sk})/P_E} \times \left(1 - \frac{P_{sk}}{P_{E,sk}}\right) \tag{5}$$

To model the multibay case, where the panel is loaded assuming uniform end shortening both before and after skin buckling so that the load effectively follows the shift in neutral axis as the skin buckles, Eqs. (4) and (5) can still be used, but with e_{sk} set to zero.

In a stiffened panel the magnitude of the skin-buckling load varies with the midlength deflection arising from the initial imperfection of the panel. The following equation is used to account for this effect:

$$P_{sk} = \frac{\sigma_{sk}}{1/A + \delta y_{sk}/I} \tag{6}$$

where A and I are the cross-sectional area and second moment of area, respectively, of the panel; y_{sk} is the distance between the neutral axis and skin midthickness of the unbuckled panel, and σ_{sk} is the skin-buckling stress for the perfect ($\delta_0 = 0$) panel. σ_{sk} can be found by using an approximation such as the following well-known equation for the buckling of a plate:

$$\sigma_{sk} = KE(t/b)^2 \tag{7}$$

where K is a suitable constant for the plate boundary conditions, E is the elastic modulus, t is the thickness of the plate, and b its width. Alternatively σ_{sk} can be obtained from an analysis of the panel using a program such as VICONOPT. For the results that follow, σ_{sk} was obtained using VICONOPT, and the values for P_E and $P_{E,sk}$ were VICONOPT overall panel-buckling loads rather than Euler loads.

III. VICONOPT Strip and Strut Model

VICONOPT[3] (VIPASA with CONstraints and OPTimization) is a FORTRAN 77 program that incorporates the earlier programs VIPASA (Vibration and Instability of Plate Assemblies including Shear and Anisotropy) and VICON (VIPASA and CONstraints). It covers any plate assembly, that is, panel of constant cross section, composed of anisotropic plates, each of which can carry any combination of uniformly distributed and longitudinally invariant in-plane stresses. It can be used as either an analysis or an optimum design program. The analysis principally covers the calculations of eigenvalues, that is, the critical load factors in elastic buckling problems or the natural frequencies in undamped vibration problems. The linear elastic buckling analysis is based on the exact solution of the governing differential equations of the constituent members, which are assumed to undergo a deformation that varies sinusoidally in the longitudinal direction yielding exact stiffness matrices whose elements are transcendental functions of load factor or frequency and the axial half-wavelength λ of the deformation. The resulting transcendental eigenproblem requires an iterative solution, which is performed using the Wittrick–Williams algorithm.[10]

VICONOPT assumes the panel to be an infinitely long (multibay) structure made up of portions, which include any supporting structures such as ribs, which repeat at longitudinal intervals l. In the simplest form of the buckling analysis,[11] the mode of buckling is assumed to vary sinusoidally in the longitudinal direction with a half-wavelength λ. The critical buckling load is taken to be the lowest buckling load found for any of a range of values of λ, extending from a value less than the smallest plate width up to the length l of the panel. If, as in this paper, the panel has no applied shear force and is fabricated from an isotropic material, then the nodal lines are necessarily straight and parallel to the panel ends. Also, because λ divides exactly into l the boundary conditions are consistent with simple supports at the ends of a panel of length l between ribs. This analysis gives reasonably accurate results for laminated and other anisotropic panels. However, for any panel carrying a significant shear load the results are conservative, particularly as $\lambda \to l$; such cases require an alternative analysis[12] that couples responses from a series of λ using Lagrangian multipliers to enforce the end conditions. To allow for continuity over the ribs with adjacent bays, warping of the entire cross section is allowed at the panel end.

For panels designed to have a postbuckling reserve, two modifications[13] have been made. First, local buckling, considered to be at any $\lambda < l$, is permitted to occur at some prescribed fraction r_L of the ultimate design load specified by the user. Second, for collapse, which can be caused by overall or torsional (stiffener) buckling, the in-plane stiffnesses of the locally buckled plates are reduced by multiplying the prebuckled stiffnesses by a factor r_s, which can be preselected by the user.[4,13] However, in this paper a separate VICONOPT postbuckling analysis[7] was performed within the optimization procedure so that values of r_s were automatically calculated for each plate in the assembly. Each value of r_s is obtained by dividing the plate stiffness after buckling by its stiffness before buckling, where each plate stiffness is obtained by dividing the average axial stress in the plate by the total axial strain at the neutral axis of the panel. The von Kármán axial strain at the neutral axis of each plate has a linear component because of the axial loading and a nonlinear component caused by flexure. Because the total strain is assumed to be uniform across the panel width, those plates subjected to the greatest flexure will carry the least axial stress, leading to low values of r_s.

When a plate is loaded axially and its longitudinal edges are required to remain straight, a nonuniform transverse stress distribution develops. This is composed of tension and compression regions, such that integration along the length gives a zero transverse stress resultant. Because the compression regions occur adjacent to the nodal lines, that is, lines of zero out-of-plane displacement, while tension regions occur around the midlength of each half-wavelength, the tension region has a greater stabilizing effect than the destabilizing effects of the compression regions. This is allowed for in VICONOPT[7] by loading the plate with a uniform (i.e., longitudinally invariant) transverse tension equal to some fraction τ of

the maximum transverse tension calculated from the postbuckling mode. The value $\tau = 0.3$ was chosen for the present work, based on previous studies on stiffened panels.[4,6] The later study[4] showed that a reduction of τ from a well-chosen value of 0.3 to a more conservative value of 0.1 decreases the failure load by less than 7%.

IV. Example Design

This section first describes the realistic example design problem that has been used to verify the postbuckled design methodology in VICONOPT. The optimum design results produced by VICONOPT are then presented before comparison with the nonlinear finite element program ABAQUS and the strut model described in Sec. II.

A. Problem Definition

The problem used here is based on practical wing data used previously[14] to demonstrate the application of VICONOPT to optimize panels that are constrained from buckling below their ultimate loads. For the work presented in the current paper, the design of a single highly loaded compression panel at a location just outboard of the engine has been considered. Here, the ultimate applied end load per unit panel width, caused by a 2.5-g maneuver case at cruise speeds with full fuel, is 3.68 kN/mm, and the corresponding limit load is $2/3 \times 3.68$ kN/mm (2.45 kN/mm). To ensure that a practical design was obtained, a stiffener pitch of 150 mm, panel length of 600 mm, and an inverted J-shaped stiffener were assumed. This geometry is in practice influenced by manufacturing constraints, and the values and cross section chosen are typical for a 150-seat, twin-engine aircraft. The material used, aluminum 7075-T6, had an elastic modulus of 74.99 GPa, Poisson's ratio of 0.33, and density of 2800 kg/m^3. In the VICONOPT and ABAQUS results that follow, the panel was modeled assuming infinite width.

B. VICONOPT Results

VICONOPT was used to produce a minimum mass design in which no initial buckling occurred below the limit load, that is, $r_L = 2/3$, and only stable postbuckled behavior occurred between limit load and ultimate load. The material was assumed to be linear-elastic.

The panel was modeled as a single repeating portion of width $b = 150$ mm with one stiffener and simply supported ends, as shown in Fig. 3. The model allowed for offsets between the centerlines of connected plates.[11] The panel was designed with VICONOPT assuming a negative bow-type imperfection of amplitude $\delta_0 = -l/1000$, which increases compression in the stiffener relative to the skin. Table 1 lists the seven independent design variables b_{fr}, b_w, b_{fa}, t_{fr}, t_w, t_{fa}, and t_s. The breadth of the unsupported skin was a dependent variable $b_s = b - 2b_{\text{fa}}$. The cross-sectional area of one stiffener is defined as $A_s = b_{\text{fr}}t_{\text{fr}} + b_w t_w + 2b_{\text{fa}}t_{\text{fa}}$, and the cross-sectional area of skin within one repeating portion equals bt_s. The cross-sectional area ratio $\gamma\,(=A_s/bt_s)$ and mass of one repeating portion are also listed in Table 1. Twenty design cycles were performed, but the panel mass had converged to within 2% of its final value after just four cycles.

Although the design was carried out without explicit constraints on strain or the value of the ratio γ, analysis of the final panel configuration confirmed that all strains remained below the assumed elastic limit of 6770 μ strain at the limit load and that γ remained in the range $0.75 \le \gamma \le 1.00$ which is typically acceptable in industry. The final design also met all of the design requirements when modeled as perfect or with a positive bow-type imperfection $\delta_0 = +l/1000$.

The first part of Table 2 lists the VICONOPT analysis results for the final panel configuration, assuming multibay conditions. For all of the imperfection cases, VICONOPT predicts initial buckling in a local mode ($\lambda = l/5$). Under further loading there is a stable postbuckling response until collapse occurs at the initiation of buckling in another (nonlocal) mode. For a positive imperfection ($\delta_0 = +l/1000$) VICONOPT predicts collapse at 3.74 kN/mm in an overall mode. For a negative imperfection ($\delta_0 = -l/1000$) VICONOPT predicts collapse at 3.65 kN/mm in a torsional mode, which will precipitate overall failure. For zero imperfection VICONOPT predicts collapse at 3.79 kN/mm in an overall mode. Thus, in each case the collapse load is near or above the design requirement of 3.68 kN/mm. Moreover, the peak strains at limit load $\varepsilon_{\text{limit}}$ are elastic. These peak strains are measured at the midsurface of the plate in which the strain occurs. The last column of Table 2 lists the ratios of postbuckled to prebuckled stiffness k^*/k for the panel. The corresponding values of r_s for each plate are listed in Table 3. It can be seen that the values for locally buckled skin

Table 1 Starting and final values of designed panel

Variable	Constraint value	Start	End
b_{fr}, mm	≥ 25	40	30.26
b_w, mm	$40 \le b_w \le 65$	65	49.02
b_{fa}, mm	$25 \le b_{\text{fa}} \le 45$	30	36.09
b_s, mm	$=150 - 2b_{\text{fa}}$	90	77.83
t_{fr}, mm	≥ 0.5	5	3.95
t_w, mm	≥ 0.5	3	4.73
t_{fa}, mm	≥ 0.5	3	1.42
t_s, mm	≥ 0.5	5	4.06
$\gamma = A_s/bt_s$,	——	0.77	0.75
Mass, kg	——	2.23	1.78

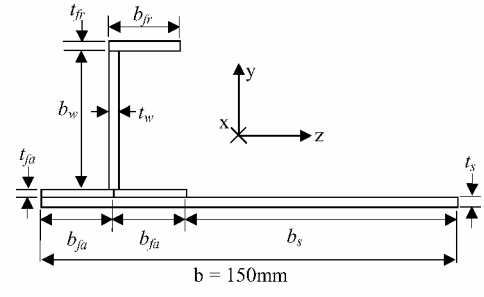

Fig. 3 Cross section of repeating portion of panel.

Table 2 Summary of VICONOPT and ABAQUS results for the final VICONOPT design showing initial buckling loads (and associated half-wavelengths) obtained using linear and nonlinear analyses, postbuckled collapse loads, collapse modes, mid surface strains at limit load $\varepsilon_{\text{limit}}$ and post-to prebuckling stiffness ratios (k^*/k) of the whole panel

		Initial buckling, kN/mm		Collapse			
Model	δ_0	Linear	Nonlinear	kN/mm	Mode	$\varepsilon_{\text{limit}}$ (μ strain)	k^*/k
VICONOPT	$+l/1000$	2.48 (l/5)	——	3.74	Overall	4800 (SK)[a]	0.68
Multibay	0	2.59 (l/5)	——	3.79	Overall	4600 (U)[b]	0.69
	$-l/1000$	2.73 (l/5)	——	3.65	Torsional	5300 (ST)[c]	0.70
ABAQUS	$+l/1000$	——	2.48 (l/5)	≈ 3.52	Overall/skin	5010 (SK)	0.53
Single-bay	0	2.63 (l/5)	2.60 (l/5)	≈ 3.57	Overall/skin	4930 (SK)	0.54
	$-l/1000$	——	2.70 (l/5)	3.63	Overall/skin	5390 (ST)	0.55
ABAQUS	$+l/1000$	——	2.51 (l/5)	3.66	Overall/skin	4893 (SK)	0.56
Double-bay	0	2.60 (l/5)	2.61 (l/5)	3.79	Overall/skin	4823 (SK)	0.63
	$-l/1000$	——	2.65 (l/5)	3.71	Torsional/overall	5542 (ST)	0.64

[a]SK = skin. [b]U = uniform. [c]ST = stiffener.

plates are lower than would be obtained by considering a plate with similar boundary conditions in isolation for the reasons outlined in Sec. III.

C. Finite Element Modeling

FE modeling was carried out using the package ABAQUS[8] to determine both the linear (bifurcation) and nonlinear[15] buckling behavior allowing comparison of the single- and double-bay FE models with VICONOPT and strut model results. Two FE models were developed, both using QUAD4 (S4R5) thin shell elements. To approximate a panel of infinite width, only two repeating portions were modeled. The δ_x, δ_y, θ_x, θ_y, and θ_z degrees of freedom at each node along one longitudinal edge (e.g., node A of Fig. 4) were set equal to corresponding degrees of freedom of the equivalent node on the other longitudinal edge of the model, for example, node B. Imperfections were modeled by adjusting the initial nodal geometry, and the mesh density was chosen so that each individual plate was at least four elements wide. This mesh was sufficiently fine to model local buckling. For the results of Secs. IV.D.1–IV.D.5, the effects of material plasticity were not considered.

1. *Single-Bay Model*

The single-bay model used 4800 elements and was similar to the one given in Ref. 4. This modeled the panel using a single longitudinal portion of length l. The panel was simply supported at the ends with the axis about which the end cross section of the panel rotates coincident with the neutral axis of the unbuckled panel. The cross-sectional geometry of skin and stiffener at the ends of the panel was prevented from deforming using multipoint constraints. Axial load was applied using point loads distributed so that the effective load axis of the panel was along the neutral axis of the unbuckled system. When the skin buckled, the load remained applied at the neutral axis of the unbuckled panel. The panel was analyzed to obtain the bifurcation buckling behavior of a perfect panel and the nonlinear behavior of both perfect and imperfect panels. The imperfect cases used a sinusoidal overall imperfection of amplitude $\delta_0 = \pm l/1000$.

2. *Double-Bay Model*

In this case a 9600-element model consisting of a portion of panel of length $2l$ was created. As shown in Fig. 4, ribs, comprising an additional 420 QUAD4 (S4R5) thin shell elements, were attached to the panel skin at $x = 0.5l$ and $1.5l$. Cutouts in the ribs allowed the stiffeners to pass freely, although, as shown in the enlarged section in Fig. 4, each stiffener was connected to a rib using two rigid multipoint constraints. This set of constraints represents the cleat used in practice to attach the rib to the upper flange of the stiffener. The side and upper edges of the ribs had clamped boundary conditions, with displacements in the x and z directions allowed. At the ends of the panel, the boundary conditions depicted in Fig. 4 were imposed. Axial load was applied using uniform end strain in the x direction at one end of the panel, with displacement in the x direction restrained at the other end. This resulted in load being applied (approximately) along the neutral axis of the panel before skin buckling and at the new neutral axis position after skin buckling. The stiffener webs at the panel ends were restrained to remain vertical using multipoint constraints. The δ_z degree of freedom was not suppressed at the ribs or panel ends so that the buckling and collapse loads would not be reduced because of the Poisson's ratio effect. The panel was analyzed to obtain the bifurcation buckling behavior for the perfect panel and the nonlinear behaviour for both perfect and imperfect panels. The imperfect cases used a global imperfection that consisted of a complete cosine wave, of amplitude δ_0, along the length of the panel $2l$. When examining the results, the behavior of the portion of length l between the ribs was considered. (A positive imperfection increases the relative compression in the skin compared with the stiffener for this portion.)

Table 3 Final panel configuration r_s values for each plate

δ_0	Remote flange	Web	Attached flange	Skin
$+l/1000$	0.99	0.98	0.87	0.10
0	0.99	0.98	0.87	0.13
$+l/1000$	0.99	0.98	0.88	0.17

D. Comparison of FE and VICONOPT Results

1. *Initial Buckling*

From the initial buckling loads given in Table 2, it can be seen that both FE models, using linear analysis, give slightly higher initial buckling loads for the perfect panel compared to the VICONOPT solution, with the double-bay model giving the closer result. This might be caused by the FE method slightly overestimating the stiffness of the panel. Both FE models predict that the panel will initially buckle with five half-wavelengths in the skin, which agrees with the VICONOPT solution.

The nonlinear estimates of the initial buckling load for the two FE models, of the perfect case, as seen in Table 2, are again slightly higher than predicted by VICONOPT. The initial buckling mode predicted is a skin mode with five half-wavelengths, matching both the VICONOPT and ABAQUS linear solutions. However, unlike the linear FE analysis, the single-bay solution now gives the best estimate, being within 0.4% of the VICONOPT solution. The double-bay nonlinear initial buckling solution is almost identical to that given by the linear analysis.

For the imperfect cases it can be seen that there is good agreement between the VICONOPT and the FE nonlinear solutions for

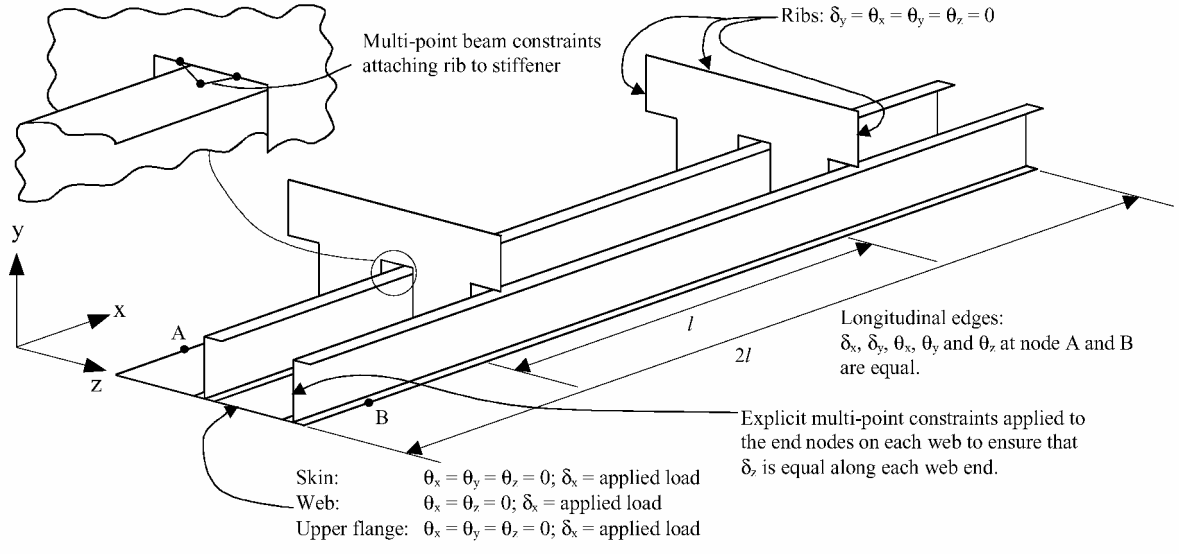

Fig. 4 Double-bay FE model showing rib and panel boundary condition and longitudinal edge conditions to approximate an infinite width panel.

initial buckling, except in the case of the $-l/1000$ solution for the ABAQUS double-bay model. Here ABAQUS predicts an initial buckling load that is about 3% lower than the VICONOPT prediction. It is thought that this is because of the shape of the negative imperfection applied to the double-bay model. This imperfection increases the compression in the skin at the ends of the panel, outside the ribs, so that these skin sections buckle early inducing buckling of the center section before it would otherwise occur. For all of the linear and nonlinear FE analyses, the initial buckling load predicted is always greater than the initial buckling load requirement of 2.45 kN/mm.

2. Collapse

The ABAQUS double-bay solutions indicate that the panel design reaches the design load (3.68 kN/mm) before collapse occurs, with the exception of the $+l/1000$ case, which can carry a load within 0.54% of the design load. The failure modes obtained by both the VICONOPT and ABAQUS double-bay solutions are similar. Both the $+l/1000$ and the perfect cases predict that failure is caused by an overall mode. With the exception of the VICONOPT perfect case, this failure mode also involves a stable interaction with the local skin-buckling mode of the type shown in Fig. 5. For the $-l/1000$ case both methods indicate that failure is caused by a $\lambda = l/2$ torsional mode, as shown in Fig. 6, which is potentially more serious as this type of failure can be unstable.

Conversely, the ABAQUS single-bay model, for all cases, predicts failure modes that are a stable interaction between the local skin and the overall buckling modes, similar to that shown in Fig. 5. Such failure modes result from the offset between the load and neutral axes that occurs when the skin buckles, as discussed in Sec. I. The effect of the offset, for the $-l/1000$ case, on the out-of-plane displacement of the single-bay model compared to the double bay model can clearly be seen in Fig. 7. These results were obtained from the average vertical displacement of the two midlength nodes

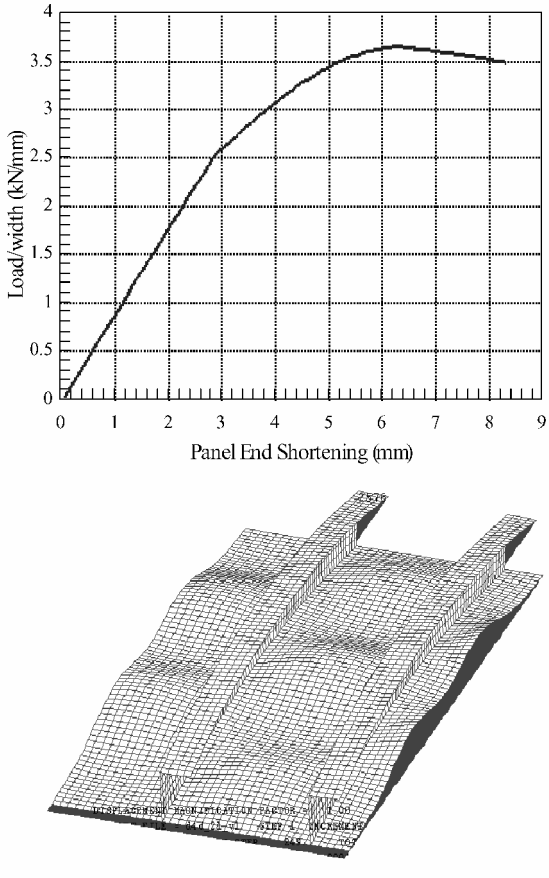

Fig. 5 End-shortening plot and final deformed shape given by ABAQUS double-bay model for the +*l*/1000 case.

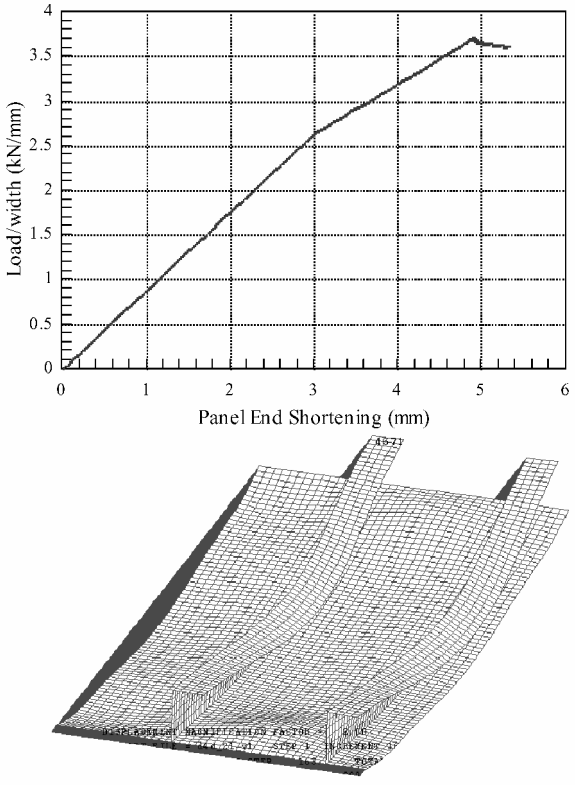

Fig. 6 End-shortening plot and final deformed shape given by ABAQUS double-bay model for the −*l*/1000 case.

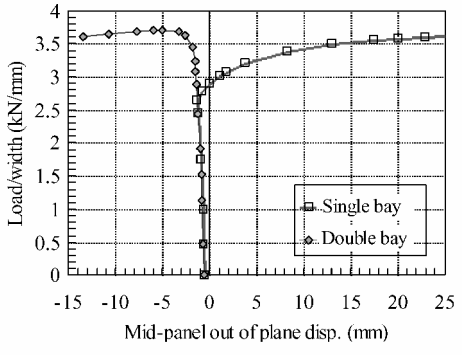

Fig. 7 Midlength out-of-plane displacement δ for the ABAQUS single-bay and double-bay models, illustrating the effect of the offset for the $\delta_0 = -l/1000$ case.

closest to the neutral axis of the unbuckled panel on each stiffener in the model. The FE single-bay solutions indicate that the design load is not reached for any imperfection case, as a result of this effect. As with the double-bay model, the $+l/1000$ case has the lowest collapse load, 4.2% below the design load. The precise collapse loads are difficult to determine for the perfect and $+l/1000$ cases as the solution became asymptotic to the overall load of the reduced stiffness panel for these cases.

3. Limit Strains

The midthickness peak strains predicted by ABAQUS at approximately the limit load are also given in Table 2. The ABAQUS strains have been given for the closest nonlinear load step to the limit load. The strain levels in the panel predicted by ABAQUS at midthickness match reasonably well the strain levels predicted by VICONOPT. Because strain is being measured at a load level where the effect of the offset in the ABAQUS single-bay model has little effect, the positions in the panel where the peak strains occur are the same for both models.

4. Stiffness Ratio

From Table 2 it can be seen that the predictions of the panel stiffness ratio (k^*/k) given by VICONOPT are 10–20% higher than those given by the ABAQUS double-bay model, where the greatest difference occurs for the positive imperfection case. This difference might be caused by the relatively high value of transverse tension factor τ that has been used for the VICONOPT postbuckling analysis. Previous work[16] has shown that reducing τ will reduce the value of k^*/k obtained, sometimes by a significant amount.

5. Out-of-Plane Displacements

Figure 8 shows the midlength out-of-plane displacement vs load behavior given by the single-bay strut model and compares this solution with the behavior predicted by the single-bay FE model. The strut model used a value of $e_{sk} = 4.334$ mm, which was calculated by assuming that the elastic modulus of the unsupported skin of the panel was multiplied by the factor $r_s = 0.133$ when the unsupported skin, width b_s, buckled (0.133 is the average of the skin stiffness reduction values given in Table 3). The overall buckling loads for the full and reduced stiffness panels P_E and $P_{E,sk}$ respectively and the skin-buckling loads for the perfect panel were obtained using VICONOPT; variation in skin-buckling loads with δ are given by Eq. (6). There is good agreement between the strut and FE models for the negative, perfect, and positive imperfections. The results confirm that failure is in the positive δ direction, that is, in an overall/skin mode in all cases. Figure 9 compares the midlength out-of-plane displacements given by the mutlibay strut model and FE double-bay model. Here, it can be seen that there are significant differences in the out-of-plane displacement predicted by the two methods after skin buckling. For the $-l/1000$ imperfection both methods predict a failure on the stiffener side, that is, in the direction of negative displacement, but the FE solutions always have more positive amplitude at a given load level than the strut model results. Because the perfect ($\delta_0 = 0$) strut model shows no out-of-plane displacement following skin buckling, as should be the case, it is evident that, as expected, the FE double-bay model approximates the true multibay conditions. To evaluate this difference, a small offset $e_{sk} = 1.1$ mm

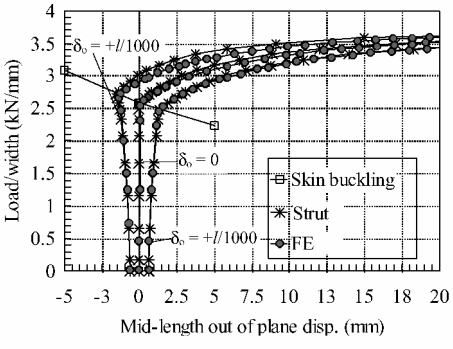

Fig. 8 Midlength out-of-plane displacement δ for the single-bay ABAQUS and strut models.

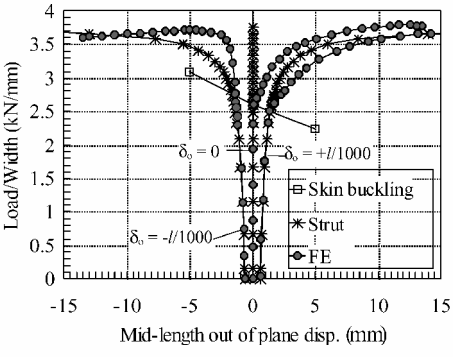

Fig. 9 Midlength out-of-plane displacement δ for the double-bay ABAQUS and multibay strut models.

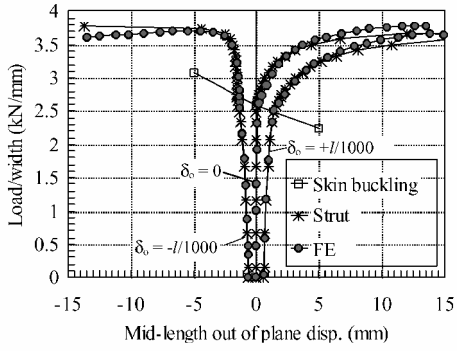

Fig. 10 Midlength out-of-plane displacement δ for double-bay ABAQUS model and strut model with e_{sk} = 1.1 mm.

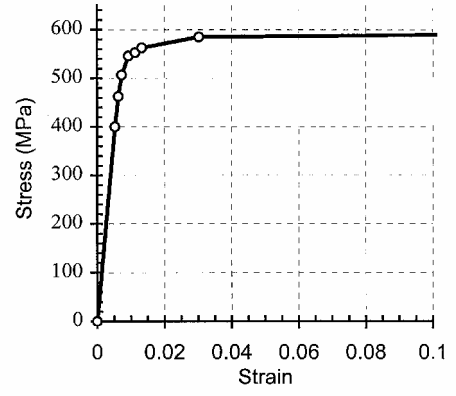

Fig. 11 Stress-strain relationship for aluminum 7075-T6.

was subsequently added to the strut model for loads above P_{sk}. This shows good agreement with the FE solution (Fig. 10). (Note that adding an additional overall imperfection term for loads above P_{sk} can instead be used to reduce the differences seen in Fig. 9, but these results are not given here.)

6. Material Plasticity

The effects of material plasticity were briefly investigated in the ABAQUS double-bay model by including the experimentally derived stress–strain relationship for aluminum 7075-T6 (Fig. 11) in the FE model. This gave initial buckling loads of 2.56 and 2.61 kN/mm for the perfect and $-l/1000$ cases, respectively, and in both cases initial buckling was in a skin mode consisting of five half-wavelengths. The primary effect of the material plasticity was on the collapse loads, which for the two cases considered occurred simultaneously with initial buckling, that is, at around 70% of the ultimate design load, indicating that the actual panel has little or no postbuckling reserve of strength. VICONOPT is currently not able to model the effects of plasticity, which are significant for the problem chosen, which is heavily loaded and has close values of initial buckling load and material yield load. A more lightly loaded panel would not be expected to present such proximity in loads. Such a panel would be designed with a thinner skin: because stiffener spacing is generally kept fixed along the wing and skin-buckling load is directly proportional to the cube of skin thickness. Thus the skin-buckling load for such a panel would be substantially lower than its yield load, which is directly proportional to skin thickness. A more lightly loaded panel would therefore be expected to exhibit linear material behavior well into the postbuckled range. Nevertheless, it is important to warn designers of the dangers of ignoring material nonlinearity when optimizing heavily loaded panels.

V. Conclusions

VICIONOPT has been used to design a panel for which skin buckling occurs at 68% of ultimate load. The assumptions made represent multibay aerospace applications, in the sense that the panel

is continuous over rib supports, and load is applied via uniform end shortening.

Comparisons of the results of an elastic VICONOPT multibay model and an elastic ABAQUS double-bay model of the preceding design indicate agreement of better than 3% on initial buckling loads and 2% on collapse loads, despite up to 20% difference between the postbuckled stiffnesses of the two models. The panel collapses in a stiffener-bucking mode when an overall sinusoidal imperfection causing increased stiffener compression is present. Such a failure is not seen in a single-bay model of the panel, indicating that there are significant phenomenological differences between postbuckling of single-, double-, and multibay panel models.

VICONOPT is suited to preliminary design, because it uses only 50 strip elements for this problem (whereas ABAQUS requires 9600 shell elements). However, the program cannot currently account for the effects of material nonlinearity.

Acknowledgments

The authors thank the Engineering and Physical Sciences Research Council (GR/M26200 and GR/M26237) and Airbus UK, Ltd., Bristol, England, United Kingdom, for providing the financial assistance that made this work possible. In addition they thank F. W. Williams and M. S. Anderson for their helpful comments.

References

[1]Dawe, D. J., Lam, S. S. E., and Azizian, Z. G., "Finite Strip Post-Local-Buckling Analysis of Composite Prismatic Plate Structures," *Computers and Structures*, Vol. 48, No. 6, 1993, pp. 1011–1023.

[2]Bushnell, D., "PANDA2—Program for Minimum Weight Design of Stiffened, Composite, Locally Buckled Panels," *Computers and Structures*, Vol. 25, No. 4, 1987, pp. 469–605.

[3]Butler, R., and Williams, F. W., "Optimum Design Using VICONOPT, a Buckling and Strength Constraint Program for Prismatic Assemblies of Anisotropic Plates," *Computers and Structures*, Vol. 43, No. 4, 1992, pp. 699–708.

[4]Lillico, M., Butler, R., Hunt, G. W., Watson, A., Kennedy, D., and Williams, F. W., "Analysis and Testing of a Post-Buckled Stiffened Panel," *AIAA Journal*, Vol. 40, No. 5, 2002, pp. 996–1000.

[5]Butler, R., Lillico, M., Hunt, G. W., and McDonald, N. J., "Experiments on Interactive Buckling in Optimized Stiffened Panels," *Proceedings of the 1st ASMO UK/ISSMO Conference on Engineering Design Optimization*, edited by V. V. Toropov, MCB Univ. Press, Bradford, England, UK, 1999, pp. 89–96.

[6]Anderson, M. S., "Inclusion of Local Post-Buckling Response in the Design of Stiffened Panels," AIAA Paper 2000-1661, 2000.

[7]Powell, S. M., Williams, F. W., Askar, A.-S., and Kennedy, D., "Local Postbuckling Analysis for Perfect and Imperfect Longitudinally Compressed Plates and Panels," *Proceedings of the 39th AIAA/ASME/ASCE/AHS/ASC Structures, Structural Dynamics, and Materials Conference*, Pt. 1, AIAA, Reston, VA, 1998, pp. 595–603.

[8]Hibbitt, Karlsson, and Sorensen, Inc., *ABAQUS/Standard User's Manual*, Ver. 5.8, Pawtucket, RI, 1999.

[9]Thompson, J. M. T., Tulk, J. D., and Walker, A. C., "An Experimental Study of Imperfection-Sensitivity in the Interactive Buckling of Stiffened Panels," *Buckling of Structures*, edited by B. Budiansky, Springer-Verlag, Berlin, 1976, pp. 149–159.

[10]Wittrick, W. H., and Williams, F. W., "A General Algorithm for Computing Natural Frequencies of Elastic Structures," *Quarterly Journal of Mechanics and Applied Mathematics*, Vol. 24, Pt. 3, 1971, pp. 263–284.

[11]Wittrick, W. H., and Williams, F. W., "Buckling and Vibration of Anisotropic or Isotropic Plate Assemblies Under Combined Loadings," *International Journal of Mechanical Sciences*, Vol. 16, No. 4, 1974, pp. 209–239.

[12]Anderson, M. S., Williams, F. W., and Wright, C. J., "Buckling and Vibration of Any Prismatic Assembly of Shear and Compression Loaded Anisotropic Plates with an Arbitrary Supporting Structure," *International Journal of Mechanical Sciences*, Vol. 25, No. 8, 1983, pp. 585–596.

[13]Anderson, M. S., "Design of Panels Having Postbuckling Strength," *Proceedings of 38th AIAA/ASME/ASCE/AHS/ASC Structures, Structural Dynamics, and Materials Conference*, Pt. 3, AIAA, Reston, VA, 1997, pp. 2407–2413.

[14]Butler, R., "Optimum Design of Composite Stiffened Wing Panels—A Parametric Study," *Aeronautical Journal*, Vol. 99, No. 985, 1995, pp. 169–177.

[15]Riks, E., "An Incremental Approach to the Solution of Snapping and Buckling Problems," *International Journal of Solids and Structures*, Vol. 15, No. 7, 1979, pp. 529–551.

[16]Powell, S. M., "Buckling and Postbuckling of Prismatic Plate Assemblies Using Exact Eigenvalue Theory," Ph.D. Dissertation, Cardiff School of Engineering, Univ. of Wales, Cardiff, Wales, U. K., Sept. 1997.

E. R. Johnson
Associate Editor